minerals

MDPI

Article

Genesis and Formation of the Tuwaishan Gold Deposit in Hainan Island, South China: Implications from H-O-S Isotopes

Yuheng Liu [1,2], Jingwen Mao [3,4,*], Jun Hu [5,6], Lei Wang [7] and Deming Xu [7]

1 MNR Key Laboratory of Geochemical Exploration, Institute of Geophysical and Geochemical Exploration, Chinese Academy of Geological Sciences, Langfang 065000, China; yuheng_liu@foxmail.com
2 UNESCO International Centre on Global-Scale Geochemistry, Langfang 065000, China
3 MNR Key Laboratory of Metallogeny and Mineral Assessment, Institute of Mineral Resources, Chinese Academy of Geological Sciences, Beijing 100037, China
4 Key Laboratory for Exploration Theory & Technology of Critical Mineral Resources, China University of Geosciences, Beijing 100083, China
5 Frontiers Science Center for Deep Ocean Multispheres and Earth System, Key Lab of Submarine Geosciences and Prospecting Techniques, MOE and College of Marine Geosciences, Ocean University of China, Qingdao 266100, China; hujun@ouc.edu.cn
6 Laboratory for Marine Mineral Resources, Qingdao National Laboratory for Marine Science and Technology, Qingdao 266237, China
7 Wuhan Center, China Geological Survey (Geosciences Innovation Center of Central South China), Wuhan 430205, China; wlei_a@mail.cgs.gov.cn (L.W.); xudeming@mail.cgs.gov.cn (D.X.)
* Correspondence: jingwenmao@263.net

Abstract: The Tuwaishan gold deposit is located at the northeastern end of the Gezhen shear zone in the western part of Hainan Island, South China. It is one of a series of similar gold deposits hosted in the Mesoproterozoic basement rocks and structurally controlled by the Gezhen shear zone. The hydrothermal ore-forming period can be divided into quartz-pyrite-arsenopyrite stage, quartz-pyrite-base metal sulfides stage and quartz-carbonate stage. Eleven gold-bearing quartz vein samples yield $\delta D_{V\text{-}SMOW}$ and $\delta^{18}O_{V\text{-}SMOW}$ values of −75.9‰ to −54.4‰ and +8.1‰ to +13.7‰, respectively, and the corresponding $\delta^{18}O_{water}$ values range from +3.1‰ to +8.7‰. In addition, the pyrite separates from 14 ore samples yield $\delta^{34}S$ values of +4.5‰ to +7.9‰. The H-O-S isotopic data, along with fluid properties of the Tuwaishan and other gold deposits along the Gezhen shear zone, suggest that the ore-forming fluid and materials are of metamorphic rather than magmatic origin. Hence, we propose that the Tuwaishan gold deposit is best classified as orogenic gold deposit that resulted from regional metamorphism. Considering that the Mesoproterozoic basement rocks have experienced amphibolite facies metamorphism prior to the gold mineralization, the metamorphic devolatilization of the Ordovician-Silurian rocks at depth would provide a realistic source of fluid, gold and sulfur for the Tuwaishan and other gold deposits of the Gezhen gold belt.

Keywords: genesis; formation; Tuwaishan gold deposit; Hainan Island; H-O-S isotopes

check for updates

Citation: Liu, Y.; Mao, J.; Hu, J.; Wang, L.; Xu, D. Genesis and Formation of the Tuwaishan Gold Deposit in Hainan Island, South China: Implications from H-O-S Isotopes. *Minerals* **2023**, *13*, 1082. https://doi.org/10.3390/min13081082

Academic Editors: Kunfeng Qiu and Victor V. Sharygin

Received: 2 June 2023
Revised: 24 July 2023
Accepted: 28 July 2023
Published: 14 August 2023

1. Introduction

Hainan Island is located in the southern margin of the South China Block, and is adjacent to the northern part of the Indochina Block [1,2] (Figure 1a). More than 50 gold deposits and occurrences have been discovered on this island, making Hainan Island a prospective region for gold exploration in South China [3–7]. The Gezhen gold belt, which consists of a series of similar gold deposits along the NE-trending Gezhen shear zone in the western Hainan Island, has become the most prospective gold exploration target within the island [4,5,8].

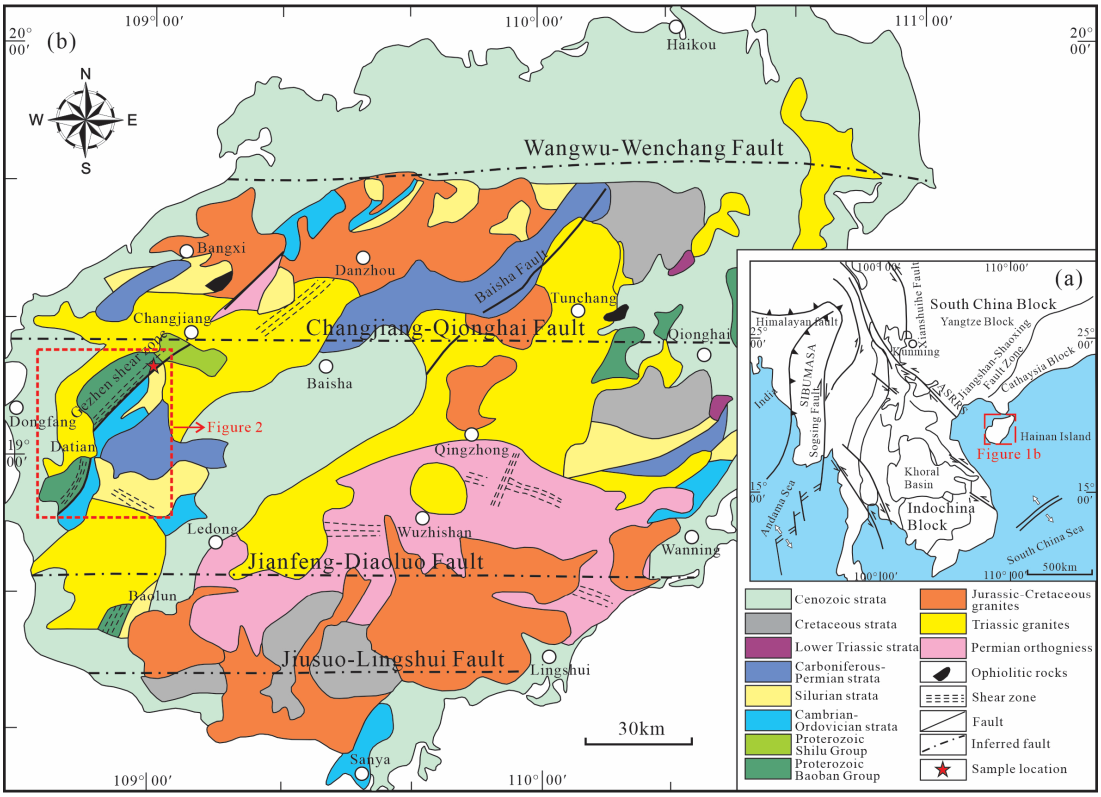

Figure 1. (**a**) Structural outline of Southeast Asia. (**b**) Simplified geological map of Hainan Island. (Revised from [9]).

Studies on ore deposit geology, ore-forming fluid characteristics and isotope compositions have been conducted to constrain the source and to further identify the genesis of the Gezhen gold deposits, but debates persist on whether those deposits are sedimentary-reworked, magmatic-hydrothermal or orogenic in genesis [5,8,10–13]. The metamorphic rocks in the Mesoproterozoic Baoban Group have long been accepted as the source of Au for the Gezhen gold belt because (1) they are the host rocks of those gold deposits and (2) they possess a relatively high content of Au [5,11,12,14–17]. However, the rocks in the Baoban Group were deposited at 1460–1430 Ma and have experienced amphibolite facies metamorphism at 1.3–1.0 Ga, whereas the Gezhen gold deposits were formed at ~243 Ma [8,18–22]. On account of the metamorphic devolatilization model, Au and sulfur would be released into the fluid phase during the prograde metamorphic transition of greenschist to amphibolite facies [23–28]. Therefore, if the Gezhen gold deposits are orogenic in genesis, then reevaluation is required for whether the regional metamorphism of the Baoban Group rocks led to the formation of the Tuwaishan and other gold deposits along the Gezhen shear zone.

In this study, we present new H-O-S isotopic compositions of ore samples from the Tuwaishan gold deposit and summarize the previously published H-O-S isotopic data for the Gezhen gold deposits to identify the source characteristics of ore-forming fluid and materials of the Tuwaishan and other gold deposits along the Gezhen shear zone. In addition, we carried out integrated analyses of source characteristics, deposit geology, regional geology of the Gezhen gold belt, as well as tectonic settings of Hainan Island to further identify the potential source for gold mineralization along the Gezhen shear zone.

2. Regional Geology

Hainan Island is separated from the mainland of South China by the Qiongzhou Strait in the north and is regarded as the southernmost extension of the Cathaysia Block [1,2,24] (Figure 1a). It is tectonically located at the junction of the Eurasian plate, the Indian–Australian plate and the Pacific plate [29–33].

The Gezhen shear zone lies between the Changjiang–Qionghai and Jianfeng–Diaoluo E-W trending faults in the western part of the Hainan Island [9] (Figure 1b). It extends for more than 55 km with a width of 0.5–3 km [34–36]. The Gezhen shear zone trends 35–40°, dips to the northwest with dip angles gradually varying from 60–80° on the surface to 15–30° with increasing depth and is characterized by both sinistral and reverse movement [9,36,37] (Figure 2). It is a multi-phase superimposed brittle-ductile shear zone and is disrupted by later NW- and E–W-trending faults [5,38] (Figure 2). The youngest shear deformation age was 227.4 ± 0.2 Ma from $^{40}Ar/^{39}Ar$ dating of synkinematic muscovite along the shear zone [9].

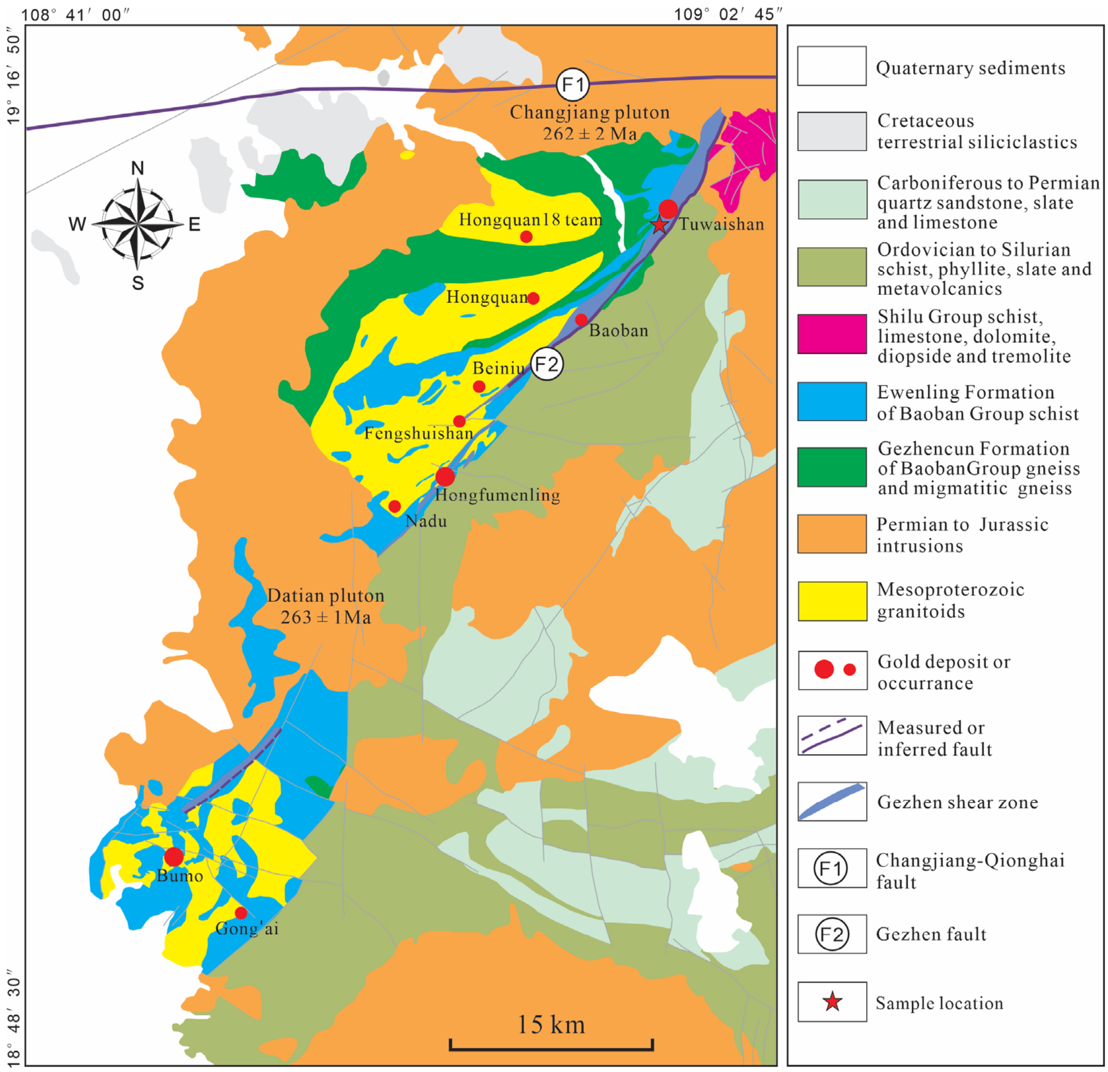

Figure 2. Geological map of the Gezhen shear zone and the Gezhen gold belt (Revised from [5]).

The hanging wall rocks of the Gezhen shear zone include the Mesoproterozoic Baoban Group and contemporaneous granitic and mafic rocks while the footwall rocks comprise the Ordovician Nanbigou Formation and the lower Silurian Tuolie Formation [20,21,39,40] (Figure 2). The Baoban Group comprising the lower Gezhencun Formation and upper Ewenling Formation was deposited at 1460–1430 Ma and suffered amphibolite facies metamorphism at 1.3–0.9 Ga [18–22]. It represents the oldest crystalline basement of the Hainan Island [37,41]. The Gezhencun Formation rocks consist of gneiss and migmatitic gneiss and have experienced migmatization and upper amphibolite facies metamorphism, while the Ewenling Formation rocks consist of quartz-mica schist, mica-quartz schist, quartzite and thin graphite layers and have experienced lower amphibolite facies metamorphism [8,19,22,37,41]. The protoliths of the Gezhencun Formation rocks are inferred to be intermediate-felsic volcanic and volcaniclastic rocks based on their whole rock geological composition while the rhythmic layering as well as relict clastic texture suggest that the protoliths of the Ewenling Formation rocks were mainly siliciclastic rocks [19,22,37,41]. The Nanbigou Formation rocks are mainly composed of quartz-mica schist, quartz-sericite phyllite and metamorphic siltstone, interspersed with metamorphic basic volcanic rocks. The overall metamorphism of the Nanbigou Formation is greenschist facies while some areas have reached upper greenschist facies metamorphism [4,42]. The low-grade metamorphic successions in the Tuolie Formation consist of phyllite, slate and metamorphic sandstone, with limestone and tuff, and the overall metamorphism is lower greenschist facies [4,42].

Magmatic rocks outcropped along the Gezhen shear zone include the Mesoproterozoic granitic and mafic rocks, as well as Middle Permian Changjiang and Datian plutons [20,21,43]. The Mesoproterozoic granitoids intruded the Baoban Group at 1450–1430 Ma, and were generally subjected to metamorphism and deformation, resulting in the formation of granitic gneiss and granitic mylonite [18,21,39,40]. The Mesoproterozoic mafic rocks were formed at 1440–1420 Ma and were metamorphosed to plagioclase amphibolite, metabasic gabbro and metabasic diabase, which are mainly lenticular, dyke and stratified in the Baoban Group [20,44]. The Datian pluton intruded the Baoban Group, Nanbitou Formation and Tuolie Formation at 263 $\pm$ 1.2 Ma [43]. It is composed of biotite monzogranite and shows gneissic schistosity within the Gezhen shear zone [43]. The Changjiang pluton consists of biotite monzogranite with a formation age of 262 $\pm$ 2.2 Ma [43].

Along the Gezhen shear zone, from NE to SW, the Tuwaishan, Baoban, Erjia and Bumo gold deposits as well as other gold deposits and occurrences have been discovered, making up the Gezhen gold belt [5,8,45–47]. Confirmed a total measured metal Au reserve of ~275 t, the Gezhen gold belt has become the most economically significant gold belt in the Hainan Island [4,5,8].

3. Deposit Geology

The Tuwaishan gold deposit is located at the northeastern end of the Gezhen shear zone, approximately 15 km southwest of the Changjiang City (Figure 2). This gold deposit was discovered during the gold rush in the Hainan Island during 1988–1991 and has been mined underground since 1997 [48]. The combined proven gold reserves and historical gold production are about 22 t at 3.5 g/t [48].

Rocks in the deposit area include quartz-mica schist of the Ewenling Formation and mylonitized Mesoproterozoic granitoids on the hanging wall, as well as schist and phyllite of the Ordovician-Silurian metamorphic successions on the footwall of the Gezhen shear zone (Figures 2 and 3). The dominant structure in the deposit area is the Gezhen shear zone. It is approximately 1.5 km in width, trends 35–40°, dips to the northwest with dip angles ranging from 60° to 80° in the mining area (Figure 3). Plagioclase amphibolites are locally observed as dykes or lenses in the Baoban Group rocks, and the dioritic porphyrites have also been found as dykes in the Mesoproterozoic metamorphic and magmatic rocks in the mining shafts [5,8,10,11]. More than 60 orebodies have been discovered in the granitic mylonites and are divided into 4 ore zones [48]. The orebodies are 150–300 m long, 5–25 m wide, strike 35–40° and dip NW from 75° on the surface to 55° with increasing depth [48].

All lenticular orebodies and gold-bearing veins are controlled by the Gezhen shear zone and its secondary fractures [5,8,47].

Two types of gold mineralization have been identified in the Tuwaishan gold deposit—disseminated ores hosted in the granitic mylonite and less common auriferous sulfide-bearing quartz veins (e.g., the smoky quartz veins; Figure 4). The granitic mylonites are the main wallrocks in the gold deposit while the mineralized quartz-mica schists and plagioclase amphibolites have also been observed. Silicification, sulfidization and sericitization have close relationships with gold mineralization while chloritization and carbonatization are also related to orebodies. Ore minerals include pyrite, arsenopyrite with lesser pyrrhotite, galena, sphalerite and chalcopyrite (Figure 5). The occurrence of gold is predominantly native gold, and electrum grains occur adjacent to or in fractures of sulfide grains and gangue minerals as free gold (Figure 5). Major gangue minerals include quartz, albite, sericite, chlorite and calcite (Figures 4 and 5).

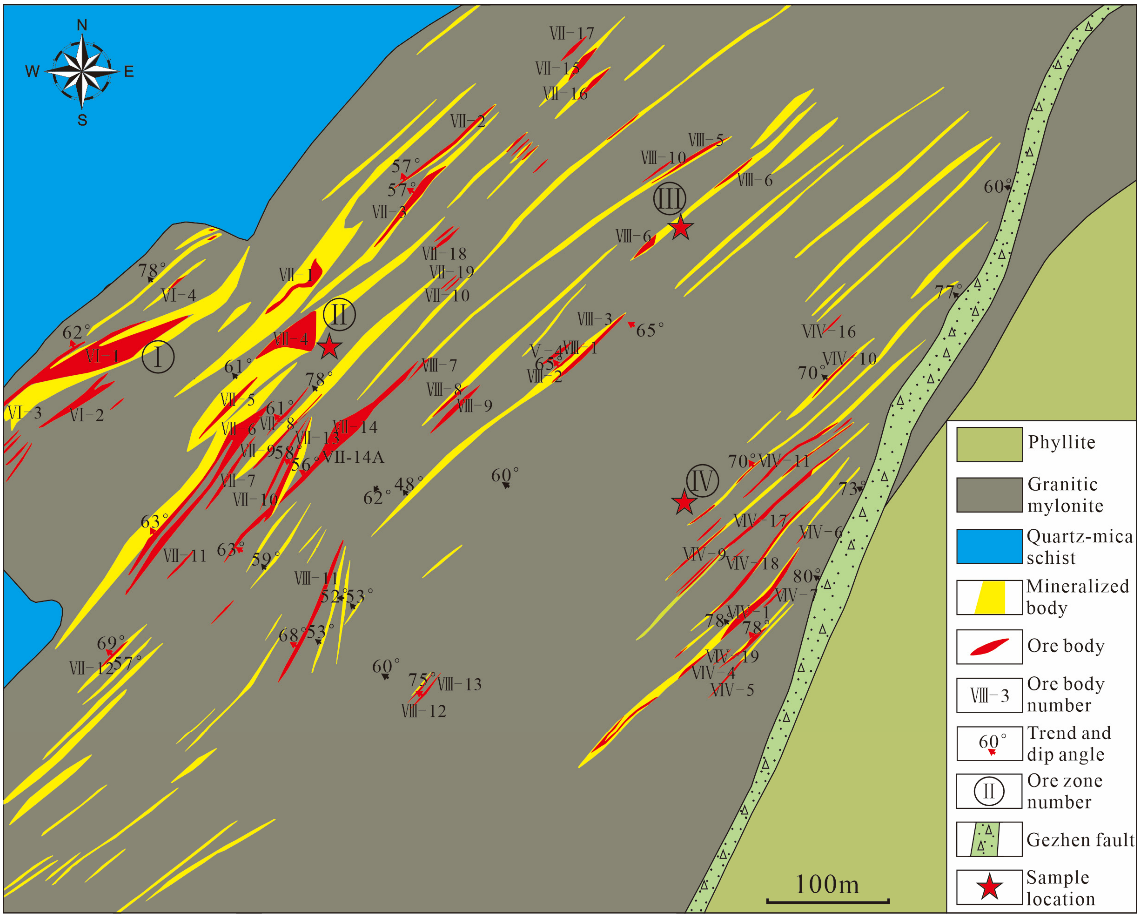

Figure 3. Mining geology of the Tuwaishan gold deposit (Revised from [47]).

Based on crosscutting relationships and mineral assemblages, the hydrothermal ore-forming period of the Tuwaishan gold deposit can be divided into three stages. The early stage gray and milky quartz veins contain pyrite, arsenopyrite, gold and local pyrrhotite (Figures 4 and 5). The middle stage is characterized by smoky quartz veins crosscutting early stage quartz veins or superimposed on the early stage silicification, containing base metal sulfides and native gold, and is the main stage for gold mineralization (Figures 4 and 5). The late stage is represented by quartz–calcite veins commonly crosscutting the earlier two stages of quartz veins with trace sulfides and almost no gold, reflecting the end of this period of ore-forming hydrothermal activity (Figure 4).

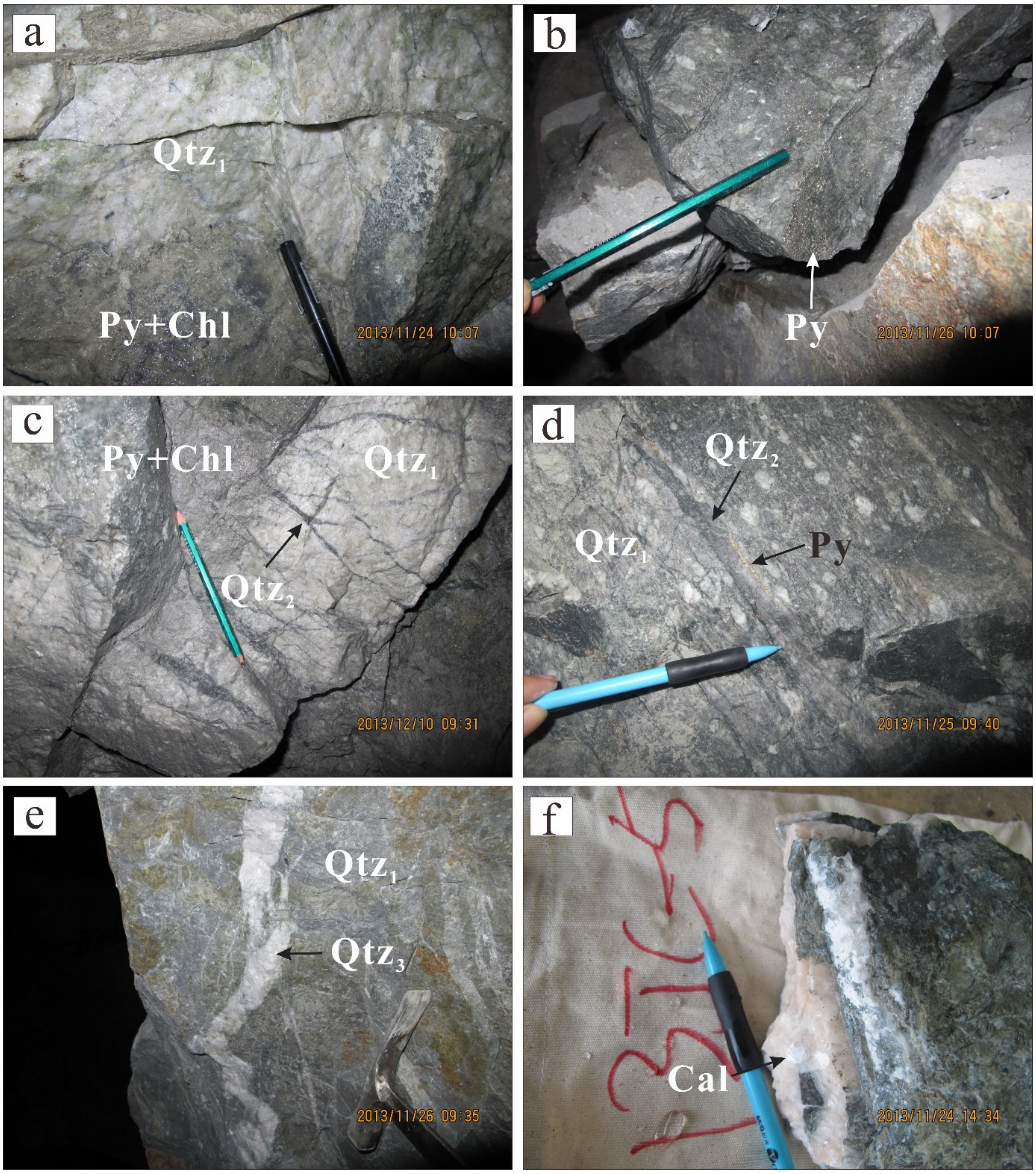

Figure 4. Wallrocks and orebodies of the Tuwaishan gold deposit. (**a**) The early stage milky quartz veins with pyrite and chlorite in alteration zones. (**b**) Disseminated ore with lots of pyrite grains. (**c**,**d**) The middle stage smoky quartz veins crosscut or superimposed on the early stage quartz veins or silicification. (**e**) The late stage barren quartz vein crosscut the earlier quartz veins. (**f**) The late stage pink calcite vein. Qtz = Quartz, Py = Pyrite, Chl = Chlorite, Cal = Calcite.

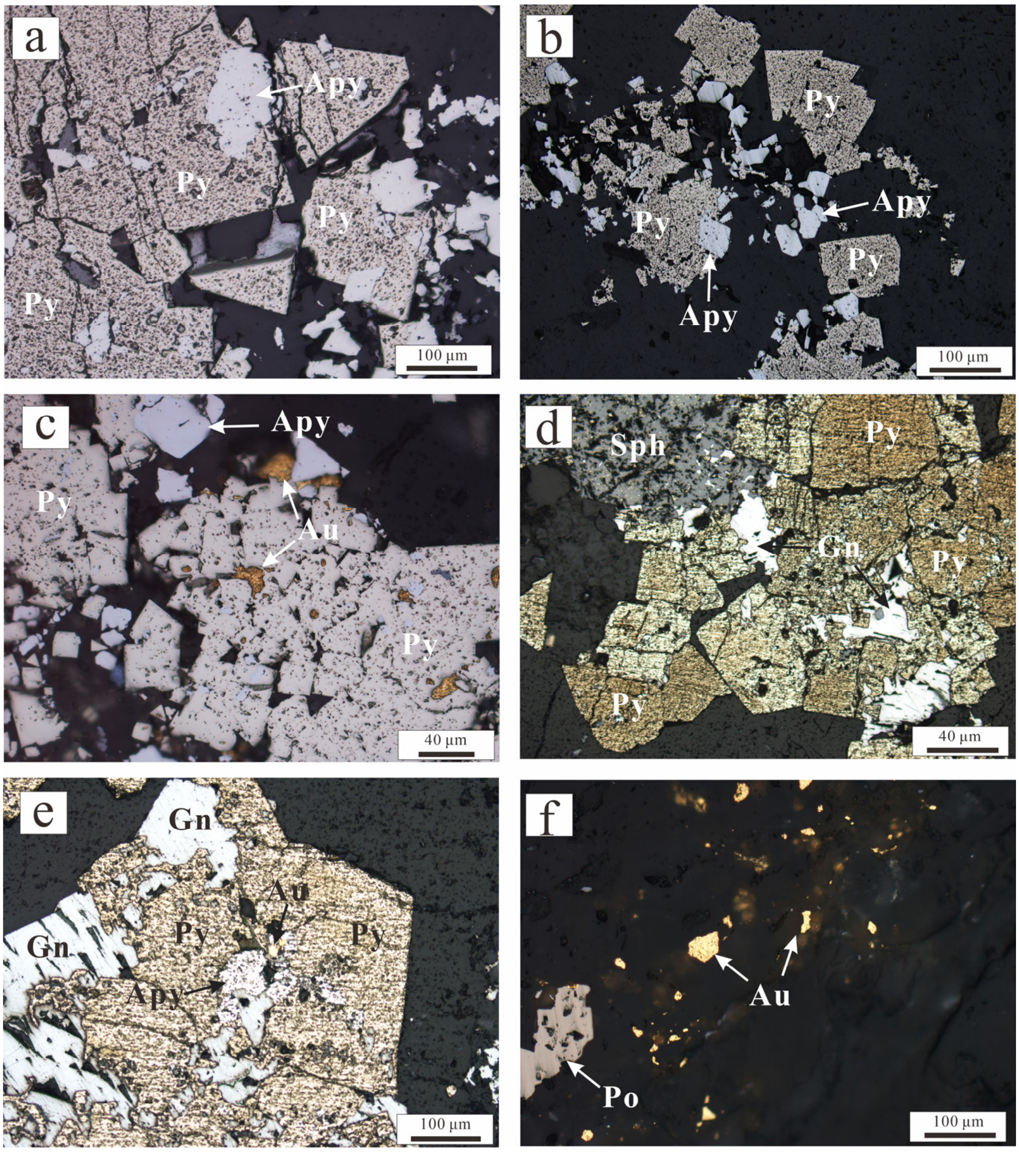

Figure 5. Alteration stages and mineral assemblages of the Tuwaishan gold deposit. (**a**,**b**) Euhedral pyrite and arsenopyrite grains with later hydrothermal alteration and deformation. (**c**) Gold grains formed in the fractures or adjacent to pyrite and arsenopyrite grains. (**d**) Pyrite, sphalerite and galena assemblage, euhedral pyrite grains altered by later sphalerite and galena. (**e**). Pyrite, arsenopyrite and galena assemblage with gold grains. (**f**). Gold grains formed in quartz grains near pyrrhotite grains. Py = Pyrite, Apy = Arsenopyrite, Po = Pyrrhotite, Gn = Galena, Sph = Sphalerite, Au = Gold.

4. Sample Description and Analytical Methods

In this study, 11 and 14 ore samples have been collected at different sections from shaft 2, 3 and 4 of the Tuwaishan gold deposit to carry out H-O and S isotope analyses, respectively. Descriptions of the samples are presented in Table 1.

Table 1. Sample location and description of the Tuwaishan gold deposit.

Number	Location	Lithology	Characteristics	Analyses
NW-7	Section 5, shaft 2	Quartz vein ore	Quartz vein with sulfides	S
JC-20	Section 5, shaft 2	Quartz vein ore	Quartz vein with sulfides	H-O
13JC-11	Section 6, shaft 3	Disseminated ore	Granitic mylonites with quartz, pyrite and chlorite	H-O-S
13JC-12	Section 6, shaft 3	Disseminated ore	Granitic mylonites with quartz, pyrite and chlorite	S
13JC-13	Section 6, shaft 3	Disseminated ore	Granitic mylonites with sulfides	S
13JC-16	Section 5, shaft 2	Disseminated ore	Granitic mylonites with sulfides	H-O-S
13JC-18	Section 5, shaft 2	Disseminated ore	Granitic mylonites with pyrite	S
13JC-19	Section 5, shaft 2	Quartz vein ore	Quartz vein with sulfides and chlorite along each sides	H-O-S
13JC-20	Section 5, shaft 2	Quartz vein ore	Quartz vein with sulfides	H-O
13JC-21	Section 5, shaft 2	Quartz vein ore	Quartz vein with sulfides	H-O
13JC-27	Section 5, shaft 3	Quartz vein ore	Quartz vein with sulfides	S
16JC-16	Section 7, shaft 3	Quartz vein ore	Quartz breccia with granitic mylonites	H-O-S
16JC-19	Section 7, shaft 3	Quartz vein ore	Smoky quartz veins with fine-grained sulfides	H-O-S
16JC-25	Section +25 m, shaft 4	Quartz vein ore	Smoky quartz veins with fine-grained sulfides	S
16JC-26	Section +25 m, shaft 4	Quartz vein ore	Smoky quartz veins with fine-grained sulfides	H-O-S
16JC-27	Section +25 m, shaft 4	Quartz vein ore	Smoky quartz veins with fine-grained sulfides	H-O-S
16JC-29	Section +25 m, shaft 4	Quartz vein ore	Smoky quartz veins with fine-grained sulfides	H-O
16JC-30	Section +25 m, shaft 4	Disseminated ore	Granitic mylonites with pyrite and chlorite	S

The H and O isotope analyses were completed at the Beijing Research Institute of Uranium Geology, China (BRIUG). Quartz grains were crushed into 40–60 mesh and further handpicked under a binocular microscope, followed by fine grinding and sieving before treatment with dehydrated ethanol to ensure a purity of better than 99% [49,50]. The H and O isotopic compositions of the purified quartz were measured using a MAT-253 gas isotope ratio mass spectrometer (Thermo Fisher Scientific, Waltham, MA, USA). Hydrogen isotope was measured on water released from fluid inclusions of the quartz via thermal decrepitating. The purified quartz samples were first degassed through heating under a vacuum at 90 °C for 12 h. Then, the water was released from fluid inclusions by heating the samples to 400–500 °C [51]. The released water was trapped and reduced to H_2 by zinc powder before analyses with gas isotope ratio mass spectrometer. Oxygen isotope analyses were based on the BrF_5 extraction technique, with O being extracted by reacting with BrF_5 [52]. The resulting O_2 was reacted with graphite rods to produce CO_2 before analyses with gas isotope ratio mass spectrometer. The isotopic results were standardized with Vienna-Standard Mean Ocean Water (V-SMOW) for H and O isotopes, while the analytical precisions were better than ±2% for δD values and ±0.2% for $\delta^{18}O$ values. The isotopic fractionation of oxygen between quartz and water was calculated using the equation of $1000\ln\alpha = 3.38 \times 10^6/T^2 - 3.4$ [52].

5. Results

The H and O isotopic compositions of gold ores from the Tuwaishan gold deposit, alone with those of the Baoban, Bumo, Erjia gold deposits as well as the wallrock granitic mylonites from previous studies are presented in Table 2 and plotted in Figure 6. The 11 ore samples of the Tuwaishan gold deposit yield $\delta D_{V\text{-}SMOW}$ and $\delta^{18}O_{V\text{-}SMOW}$ values from −75.9‰ to −54.4‰ and from +8.1‰ to 13.7‰, respectively. Given 360 °C as the trapping temperature for the main stage of gold mineralization of the Tuwaishan gold deposit [47], the corresponding $\delta^{18}O_{water}$ values range from +3.1‰ to +8.7‰.

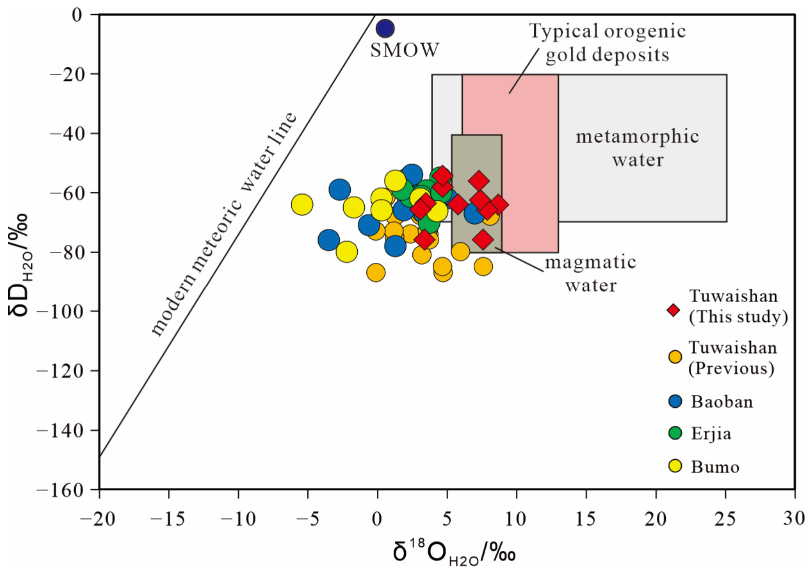

Figure 6. Plot of δD versus calculated $\delta^{18}O_{water}$ for quartz veins of the Gezhen gold deposits. Base map modified after [43]. Magmatic water, metamorphic water and meteoric water line are from [53]. Hydrogen and oxygen isotopic compositions of typical orogenic gold deposits are from [54].

Table 2. Hydrogen and oxygen isotopic data of quartz veins from the Gezhen gold deposits.

Gold Deposit	Sample Number	Lithology	Mineral	$\delta^{18}O_{SMOW}$ (‰)	$\delta^{18}O_{H2O}$ (‰)	δD_{SMOW} (‰)	Equilibrium Temperature (°C)	Data Source
Tuwaishan	16JC-16	Gold ore	Quartz	8.5	3.5	−63.6	360	This study
Tuwaishan	16JC-19	Gold ore	Quartz	12.6	7.6	−75.9	360	This study
Tuwaishan	16JC-26	Gold ore	Quartz	13.7	8.7	−64.2	360	This study
Tuwaishan	16JC-27	Gold ore	Quartz	12.9	7.9	−65.9	360	This study
Tuwaishan	16JC-29	Gold ore	Quartz	10.8	5.8	−64.0	360	This study
Tuwaishan	13JC-11	Gold ore	Quartz	8.4	3.4	−75.9	360	This study
Tuwaishan	13JC-16	Gold ore	Quartz	8.1	3.1	−65.8	360	This study
Tuwaishan	JC-20	Gold ore	Quartz	12.4	7.4	−62.6	360	This study
Tuwaishan	13JC-19	Gold ore	Quartz	9.7	4.7	−58.2	360	This study
Tuwaishan	13JC-20	Gold ore	Quartz	9.7	4.7	−54.4	360	This study
Tuwaishan	13JC-21	Gold ore	Quartz	12.3	7.3	−56.2	360	This study
Tuwaishan	2-4-B1	Gold ore	Quartz	13.0	3.7	−74.0	252	Yang, 2008 [13]
Tuwaishan	2-4-B2	Gold ore	Quartz	14.8	6.0	−80.0	253	Yang, 2008 [13]
Tuwaishan	2-4-B3	Gold ore	Quartz	15.0	7.6	−85.0	287	Yang, 2008 [13]
Tuwaishan	2-4-A3	Gold ore	Quartz	15.3	4.7	−87.0	238	Yang, 2008 [13]
Tuwaishan	3-A1	Gold ore	Quartz	14.3	3.2	−81.0	211	Yang, 2008 [13]
Tuwaishan	3-A3	Gold ore	Quartz	14.4	2.4	−74.0	195	Yang, 2008 [13]
Tuwaishan	3-A5	Gold ore	Quartz	15.0	3.6	−73.0	224	Yang, 2008 [13]
Tuwaishan	3-A4	Gold ore	Quartz	14.9	3.8	−76.0	209	Yang, 2008 [13]
Tuwaishan	2-4-C1	Gold ore	Quartz	12.1	1.3	−75.0	214	Yang, 2008 [13]
Tuwaishan	2-4-C2	Gold ore	Quartz	12.5	1.3	−68.0	208	Yang, 2008 [13]
Tuwaishan	TIV-2	Gold ore	Quartz	12.1	3.1	−67.8	252	Hou et al., 1996 [16]
Tuwaishan	TIV-3	Gold ore	Quartz	9.6	0.6	−61.7	252	Hou et al., 1996 [16]
Tuwaishan	T-02	Gold ore	Quartz	14.2	8.1	−68.0	323	Xiao, 1989 [55]
Tuwaishan	T-179	Gold ore	Quartz	10.9	4.7	−85.0	320	Xiao, 1989 [55]
Tuwaishan	T-09	Gold ore	Quartz	11.5	4.4	−61.9	293	Xiao, 1989 [55]
Tuwaishan	T-05	Gold ore	Quartz	13.1	2.1	−61.9	212	Xiao, 1989 [55]
Tuwaishan	T-021	Gold ore	Quartz	15.1	3.1	−66.8	196	Xiao, 1989 [55]

Table 2. *Cont.*

Gold Deposit	Sample Number	Lithology	Mineral	$\delta^{18}O_{SMOW}$ (‰)	$\delta^{18}O_{H2O}$ (‰)	δD_{SMOW} (‰)	Equilibrium Temperature (°C)	Data Source
Tuwaishan	T-35	Gold ore	Quartz	12.8	1.2	−73.0	200	Xiao, 1989 [55]
Tuwaishan	T-56	Gold ore	Quartz	10.2	−0.1	−87.0	220	Xiao, 1989 [55]
Tuwaishan	V2-3	Gold ore	Quartz	13.7	−0.1	−73.0	171	Feng, 1989 [56]
Tuwaishan	V5-161	Gold ore	Quartz	10.7	2.1	−55.0	259	Feng, 1989 [56]
Tuwaishan	V102-05	Gold ore	Quartz	13.1	2.1	−62.0	212	Feng, 1989 [56]
Baoban	PV1-1	Gold ore	Quartz	10.0	2.7	−61.0	290	Chen et al., 1993 [11]
Baoban	PV1-2	Gold ore	Quartz	9.8	2.5	−54.0	290	Chen et al., 1993 [11]
Baoban	B249	Gold ore	Quartz	7.5	−3.5	−76.0	210	Xiao, 1989 [55]
Baoban	B279	Gold ore	Quartz	10.3	−2.7	−59.0	180	Xiao, 1989 [55]
Baoban	V1-9-3	Gold ore	Quartz	10.2	1.9	−66.0	265	Feng, 1989 [56]
Baoban	V1-8-8	Gold ore	Quartz	11.1	1.3	−78.0	234	Feng, 1989 [56]
Baoban	V1-8-1	Gold ore	Quartz	11.3	−0.6	−71.0	197	Feng, 1989 [56]
Baoban	V101-021	Gold ore	Quartz	16.1	3.4	−67.0	200	Feng, 1989 [56]
Baoban	V101-09	Gold ore	Quartz	11.5	4.4	−62.0	292	Feng, 1989 [56]
Baoban	021	Gold ore	Quartz	15.1	7.0	−67.0	280	Feng, 1989 [56]
Baoban	09	Gold ore	Quartz	11.5	3.4	−62.0	280	Feng, 1989 [56]
Baoban	05	Gold ore	Quartz	13.1	5.0	−62.0	280	Feng, 1989 [56]
Erjia	J107-1	Gold ore	Quartz	13.1	4.2	−64.2	250	Chen, 1996 [57]
Erjia	J107-3	Gold ore	Quartz	13.5	4.5	−55.0	250	Chen, 1996 [57]
Erjia	J107-6	Gold ore	Quartz	12.7	3.7	−70.2	250	Chen, 1996 [57]
Erjia	J107-8	Gold ore	Quartz	12.5	3.6	−59.3	250	Chen, 1996 [57]
Erjia	J107-10	Gold ore	Quartz	11.3	2.4	−61.4	250	Chen, 1996 [57]
Erjia	J107-11	Gold ore	Quartz	12.1	3.2	−61.2	250	Chen, 1996 [57]
Erjia	A58	Gold ore	Quartz	10.4	1.8	−59.0	270	Tu and Gao, 1993 [12]
Erjia	A66	Gold ore	Quartz	13.2	4.6	−60.0	270	Tu and Gao, 1993 [12]
Bumo	BM4-1	Gold ore	Quartz	12.2	4.3	−66.3	280	Hou et al., 1996 [16]
Bumo	B3-7	Gold ore	Quartz	8.8	0.3	−62.0	270	Tu and Gao, 1993 [12]
Bumo	B4	Gold ore	Quartz	11.6	3.1	−62.0	270	Tu and Gao, 1993 [12]
Bumo	B10	Gold ore	Quartz	8.1	−5.4	−64.0	180	Tu and Gao, 1993 [12]
Bumo	B11	Gold ore	Quartz	11.9	−1.7	−65.0	180	Tu and Gao, 1993 [12]
Bumo	B20	Gold ore	Quartz	9.4	−2.2	−80.0	210	Tu and Gao, 1993 [12]
Bumo	B25	Gold ore	Quartz	9.8	1.3	−56.0	270	Tu and Gao, 1993 [12]
Bumo	B26	Gold ore	Quartz	8.8	0.3	−66.0	270	Tu and Gao, 1993 [12]

The S isotope data of pyrites from the Gezhen gold deposits as well wallrocks and dykes are listed in Table 3 and plotted in Figure 7. The 14 ore samples of the Tuwaishan gold deposit show $\delta^{34}S$ values of +4.5‰ to +7.9‰ with a narrow variation of 3.4‰ and an average of +6.3‰.

Table 3. Sulfur isotopic data of pyrites from the Gezhen gold deposits, wallrocks, intrusions and dykes.

Gold Deposit	Sample Number	Lithology	Mineral	$\delta^{34}S$‰	Sample Size	Data Source
Tuwaishan	NW-7	Gold ore	Pyrite	5.0		This study
Tuwaishan	13JC-11	Gold ore	Pyrite	4.5		This study
Tuwaishan	13JC-12	Gold ore	Pyrite	7.1		This study
Tuwaishan	13JC-13	Gold ore	Pyrite	6.9		This study
Tuwaishan	13JC-16	Gold ore	Pyrite	7.0		This study
Tuwaishan	13JC-18	Gold ore	Pyrite	6.8		This study
Tuwaishan	13JC-19	Gold ore	Pyrite	7.5		This study
Tuwaishan	13JC-27	Gold ore	Pyrite	4.5		This study
Tuwaishan	16JC-16	Gold ore	Pyrite	7.1		This study

Table 3. *Cont.*

Gold Deposit	Sample Number	Lithology	Mineral	$\delta^{34}S$‰	Sample Size	Data Source
Tuwaishan	16JC-19	Gold ore	Pyrite	6.1		This study
Tuwaishan	16JC-25	Gold ore	Pyrite	7.9		This study
Tuwaishan	16JC-26	Gold ore	Pyrite	6.5		This study
Tuwaishan	16JC-27	Gold ore	Pyrite	6.8		This study
Tuwaishan	16JC-30	Gold ore	Pyrite	5.0		This study
Tuwaishan	No.1	Gold ore	Pyrite	6.3		Hou et al., 1996 [16]
Tuwaishan	No.6	Gold ore	Pyrite	6.4		Hou et al., 1996 [16]
Tuwaishan	TV-IV	Gold ore	Pyrite	6.8		Hou et al., 1996 [16]
Tuwaishan	Tj-21	Gold ore	Pyrite	6.4		Hou et al., 1996 [16]
Tuwaishan	T-55	Gold ore	Pyrite	5.2		Hou et al., 1996 [16]
Tuwaishan	T-90-2	Gold ore	Pyrite	6.5		Hou et al., 1996 [16]
Tuwaishan	T-35	Gold ore	Pyrite	6.1		Hou et al., 1996 [16]
Tuwaishan	T-90-1	Gold ore	Pyrite	6.1		Hou et al., 1996 [16]
Tuwaishan	T-54	Gold ore	Pyrite	7.1		Hou et al., 1996 [16]
Tuwaishan	T-56	Gold ore	Pyrite	5.6		Hou et al., 1996 [16]
Tuwaishan	T-27	Gold ore	Pyrite	6.7		Hou et al., 1996 [16]
Tuwaishan	B-249	Gold ore	Pyrite	8.2		Hou et al., 1996 [16]
Tuwaishan		Gold ore	Pyrite	5.0–8.2	Unknown	Liang, 1992 [10]
Tuwaishan		Gold ore	Pyrite	4.0–8.2	10	Xia, 2002 [17]
Baoban	P202	Gold ore	Pyrite	6.7		Tu and Gao, 1993 [12]
Baoban	BV30-1	Gold ore	Pyrite	6.7		Hou et al., 1996 [16]
Baoban	B-470	Gold ore	Pyrite	4.0		Hou et al., 1996 [16]
Erjia	J107-3	Gold ore	Pyrite	6.4		Chen, 1996 [57]
Erjia	R5-1	Gold ore	Pyrite	6.5		Chen, 1996 [57]
Erjia	R5-2	Gold ore	Pyrite	6.0		Chen, 1996 [57]
Erjia	R1-1	Gold ore	Pyrite	5.1		Chen, 1996 [57]
Erjia	R1-2	Gold ore	Pyrite	5.1		Chen, 1996 [57]
Erjia	R2-1	Gold ore	Pyrite	3.2		Chen, 1996 [57]
Erjia	R2-2	Gold ore	Pyrite	3.6		Chen, 1996 [57]
Erjia	A16	Gold ore	Pyrite	6.8		Tu and Gao, 1993 [12]
Erjia	A19	Gold ore	Pyrite	6.5		Tu and Gao, 1993 [12]
Erjia	A22	Gold ore	Pyrite	7.4		Tu and Gao, 1993 [12]
Erjia	A24	Gold ore	Pyrite	7.2		Tu and Gao, 1993 [12]
Erjia	A25	Gold ore	Pyrite	6.7		Tu and Gao, 1993 [12]
Erjia	A32	Gold ore	Pyrite	6.9		Tu and Gao, 1993 [12]
Erjia	A34	Gold ore	Pyrite	7.5		Tu and Gao, 1993 [12]
Erjia	A62	Gold ore	Pyrite	7.6		Tu and Gao, 1993 [12]
Erjia	HR34	Gold ore	Pyrite	6.8		Tu and Gao, 1993 [12]
Erjia	HR35	Gold ore	Pyrite	6.6		Tu and Gao, 1993 [12]
Erjia	EJV-23	Gold ore	Pyrite	4.1		Hou et al., 1996 [16]
Erjia		Gold ore	Pyrite	3.4–7.7	13	Xia, 2002 [17]
Bumo	B4	Gold ore	Pyrite	4.4		Tu and Gao, 1993 [12]
Bumo	B4-1	Gold ore	Pyrite	4.2		Tu and Gao, 1993 [12]
Bumo		Gold ore	Pyrite	4.3–6.4	7	Xia, 2002 [17]
Erjia		Baoban Group rocks	Pyrite	3.7–6.8	5	Huang and Ding, 1992 [14]
Tuwaishan	TyD3-5	Granitic mylonites	Pyrite	7.8		Hou et al., 1996 [16]
Tuwaishan	TyD3-6	Granitic mylonites	Pyrite	6.2		Hou et al., 1996 [16]
Tuwaishan	No.21	Granitic mylonites	Pyrite	8.5		Hou et al., 1996 [16]
Erjia	Ej-13	Granitic mylonites	Pyrite	8.2		Hou et al., 1996 [16]
Tuwaishan		Granitic mylonites	Pyrite	4.1–7.8	Unknown	Liang, 1992 [10]

Table 3. *Cont.*

Gold Deposit	Sample Number	Lithology	Mineral	$\delta^{34}S$‰	Sample Size	Data Source
Erjia		Granitic mylonites	Pyrite	2.4–8.2	10	Huang and Ding, 1992 [14]
Erjia		Metamorphic basic rocks	Pyrite	7.9		Chen et al., 1993 [11]
Tuwaishan		Metamorphic basic rocks	Pyrite	7.4–7.9	Unknown	Liang, 1992 [10]
Erjia		Diorite porphyrite dykes	Pyrite	6.9		Chen et al., 1993 [11]
Baoban	P103	Diorite porphyrite dykes	Pyrite	6.9		Hou et al., 1996 [16]
Tuwaishan		Diorite porphyrite dykes	Pyrite	2.6–3.7	3	Liang, 1992 [10]

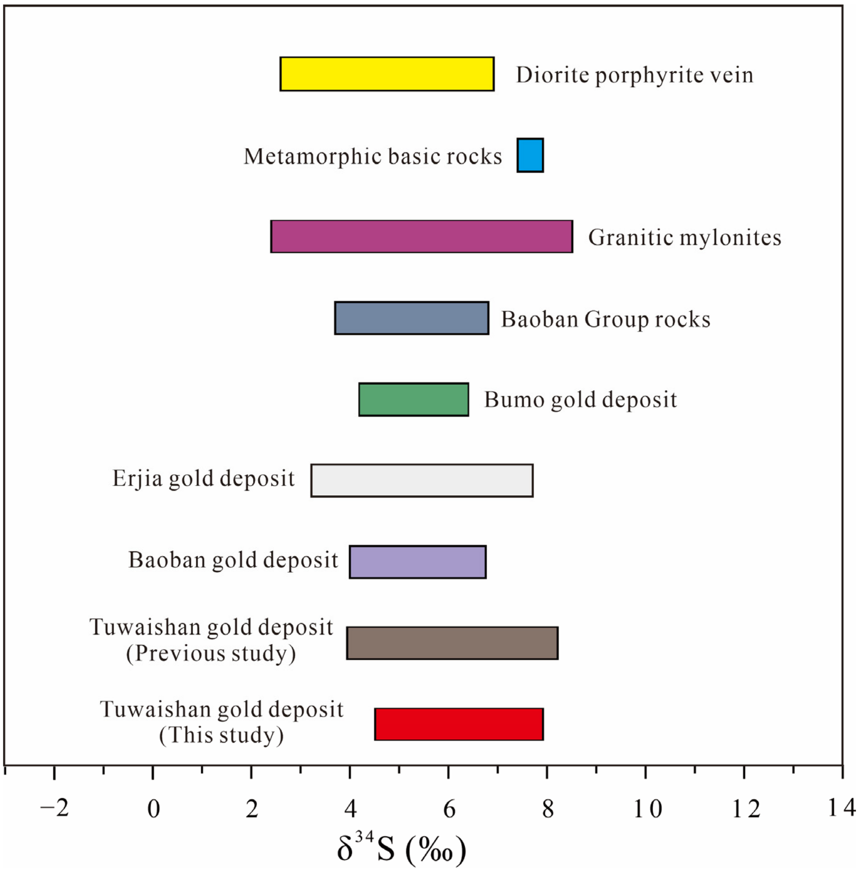

Figure 7. Comparison of sulfur isotopic compositions of the Gezhen gold deposits with wallrocks, intrusions and dykes.

6. Discussion

6.1. Ore-Forming Fluid Source

Many workers have carried out H-O isotope analyses to constrain the fluid source of the Gezhen shear zone gold deposits, and it has been proposed that a mixture of magmatic water and metamorphic water with variable contents of meteoric water are most likely the source for the Gezhen gold deposits [5,10–12,14]. The $\delta D_{V\text{-}SMOW}$ and calculated $\delta^{18}O_{water}$

values are from −87.0‰ to −55.0‰ and from −0.1‰ to +8.1‰ for the Tuwaishan gold deposit [13,16,55,56], indicating a hybrid source for ore-forming fluid [53]. Some researchers proposed that the ore-forming fluid of the Tuwaishan gold deposit originated from a mixture of magmatic water and meteoric water [10,13], while some other researchers argued that a mixture of metamorphic and meteoric water with lesser contribution of magmatic water could be the source fluid for this deposit [17].

Our new H-O isotopic data for quartz grains separated from 11 ore samples of the Tuwaishan gold deposit predominantly fall into either the metamorphic water field or the magmatic water field or the overlap zone between them in the δD_{H2O} vs. $\delta^{18}O_{H2O}$ plot (Figure 6), indicating a mixture of metamorphic and magmatic water for the ore-forming fluid source [53,58–60]. Meanwhile, half of our new data fall into the typical orogenic gold fluid field in the δD_{H2O} vs. $\delta^{18}O_{H2O}$ plot [54], suggesting the involvement of metamorphic water in the formation of the Tuwaishan gold deposit [24,54,61,62]. The ore-forming fluid of the Gezhen gold deposits is characterized as medium temperature (200–380 °C), low salinity (predominantly 3.0%–7.0%NaCleqv), reducing (H_2S exists in the gas phase composition) and CO_2 rich [12,13,15,47,63]. It is compatible with metamorphic fluid but is significantly different from the magmatic fluid [64–67]. Thus, combined with ore-forming fluid properties and H-O isotopic compositions, it is proposed that the ore-forming fluid of the Tuwaishan gold deposit is most likely sourced from metamorphic water.

6.2. Sulfur Source

Although there are plenty of available sulfur isotopic data for the Gezhen gold deposits as well as the wallrocks, intrusions and dykes (Table 3, Figure 7), debates still exist for the sulfur source of the Gezhen gold deposits. This is partly because the similarity among $\delta^{34}S$ values of the gold deposits, the Baoban Group metamorphic rocks, the granitic mylonites and the diorite porphyrite dykes (Table 3, Figure 7). Some researchers suggest that the sulfur was sourced from the magmatic fluid which has interacted with wallrocks of the Baoban Group metamorphic rocks or the granitic mylonites during its ascending, as the positive $\delta^{34}S$ values of the Gezhen gold deposits are slightly higher than those of the magmatic fluid, and are close to those of the wallrocks [10,16] (Table 3; Figure 7). However, some other workers believe that the sulfur was originated from the metamorphism of the Baoban Group rocks [12,17,68]. The indistinctive positive $\delta^{34}S$ values are not fully consistent with either magmatic fluid or sedimentary fluid [12]. In addition, the narrow variation of $\delta^{34}S$ values for the Gezhen gold deposits indicates a sulfur isotope homogenization during regional metamorphism [10,17,69–71]. Considering the high gold content of the Baoban Group rocks as well as their close spatial relationship with the Gezhen gold deposits, many researchers believe that the metamorphism of the Baoban Group rocks played a key role in the formation of those gold deposits [12,16,17,68].

Field and microscopic observations suggest that ore minerals of the Gezhen gold deposits are predominantly sulfides including pyrite, arsenopyrite, sphalerite, galena and chalcopyrite whereas sulfates are absent [16,47]. Thus, the sulfur isotope compositions of sulfides should be approximately the same as those of the ore-forming fluid [69,72]. Our new $\delta^{34}S$ values of pyrite separates from 14 ore samples from the Tuwaishan gold deposit show positive values (from +4.5‰ to +7.9‰) with a narrow variation (3.4‰), which strongly imply a sulfur isotope homogenization caused by regional metamorphism during the formation of the gold deposit [27,54,70]. Furthermore, the same $\delta^{34}S$ values among the Tuwaishan, Baoban, Erjia and Bumo gold deposits request a common source for all gold deposits along the Gezhen shear zone (Table 3; Figure 7). Thus, the plagioclase amphibolites as well as the diorite porphyrite dykes are not likely the sources of sulfur for the Gezhen gold deposits due to their scattered distribution and limited scales [5,16]. It is concluded that the sulfur of the Tuwaishan gold deposit, as well as other gold deposits along the Gezhen shear zone, is originated from regional metamorphism of sources rocks.

6.3. Genesis and Formation of the Tuwaishan Gold Deposit

The Gezhen gold deposits have been traditionally classified as sedimentary-reworked [10–12] or magmatic-hydrothermal origin [13]. Xu et al. [5] summarized previous studies on deposit geology, ore-forming fluid characteristics and isotope compositions of the Gezhen gold deposits and concluded that these gold deposits were best classified as orogenic in genesis. Our new data on H-O-S isotopic compositions of the Tuwaishan gold deposit further support the orogenic gold classification not only because the H-O-S isotopic compositions of the Tuwaishan gold deposit are consistent with those of typical orogenic gold deposits worldwide [6,54,73,74] (Figures 6 and 7) but also because the comprehensive interpretations of our new H-O-S isotopic data with ore-forming fluid properties favor a metamorphic rather than a magmatic origin.

As discussed above, the Tuwaishan gold deposit belongs to orogenic gold deposit and is most likely sourced from metamorphism. Therefore, the host rocks of the Baoban Group metamorphic rocks are seemingly the potential sources of both ore-forming fluid and materials for the Tuwaishan gold deposit as well as other gold deposits along the Gezhen shear zone. In fact, it has been widely accepted by early researchers on Hainan gold deposits that the Baoban Group rocks are the source rocks for the Gezhen gold deposits [5,11,12,14–17]. Accordingly, it has been proposed that the metamorphic fluid released from regional metamorphism of the Baoban Group rocks mixed with magmatic fluid or the magmatic fluid that extracted Au from the Baoban Group rocks during its ascending, which deposited Au and sulfides in appropriate spaces in the Gezhen shear zone, is the major mechanism of gold mineralization along the shear zone [11,16,17].

However, despite the fact that the Gezhen gold deposits were sourced from metamorphism, and the Baoban Group metamorphic rocks are the host rocks, those Mesoproterozoic basement rocks are not necessarily the source for the Gezhen gold deposits [8]. Based on the metamorphic devolatilization model for orogenic gold deposits, most of sulfur and Au would have been released from the source rocks into the metamorphic fluid during the prograde metamorphic transition from the greenschist to the amphibolite facies [23,24,75–77]. This is when the source rocks were first heated through a temperature-pressure window that broke chlorite, pyrite, organic matter and various other minerals and contributed to the fluid phase [24]. The Baoban Group rocks together with the Mesoproterozoic mafic rocks have experienced amphibolite facies regional metamorphism at 1.3–0.9 Ga [18,19,22], during which time those Mesoproterozoic basement rocks have lost most of their Au and sulfur [8,24,54,77]. Therefore, the Baoban Group rocks could not be a source for the fluid and gold for the gold mineralization at ca. 243 Ma along the Gezhen shear zone [8]. Instead, The Ordovician Nanbigou Formation rocks and the Silurian Tuolie Formation rocks on the footwall of the Gezhen shear zone have experienced greenschist facies and lower greenschist facies regional metamorphism, respectively [4,42]. Even through the timing and duration for this metamorphism have not been well constrained, the continuous amalgamation process from back-arc consumption (272–252 Ma) to orogenic assembly (251–243 Ma) between the South China and Indochina Blocks represents an important tectono-thermal event that would promote regional metamorphism in Hainan Island [2,8,78]. Considering the fact that the Ordovician–Silurian rocks are on the footwall of the reverse Gezhen shear zone (Figure 2), and the dip angle gradually decreases with increasing depth [9,36], metamorphic devolatilization of these rocks at depth would provide a realistic source of fluid, gold and sulfur for the gold mineralization along the shear zone. Therefore, we propose that the Ordovician–Silurian rocks on the footwall of the Gezhen shear zone are most likely the sources of ore-forming fluid and materials for the Tuwaishan gold deposit and other gold deposits along the Gezhen shear zone.

7. Conclusions

New H-O-S isotopic data of the Tuwaishan gold deposit in Hainan Island are reported here. In combination with H-O-S isotopic compositions and ore-forming fluid properties of the Gezhen gold deposits from previous works, this study identified the ore-forming fluid and material source characteristics of the Tuwaishan and other gold deposits along the Gezhen shear zone. Furthermore, with integrated studies on source characteristics, deposit geology and regional geology of the Gezhen gold deposits, as well as tectonic settings of Hainan Island, a realistic source has been proposed for the Tuwaishan and other gold deposits along the Gezhen shear zone. The main conclusions are as follows:

(1) The δD and $\delta^{18}O$ values for ore-forming fluid of the Tuwaishan gold deposit are from −75.9‰ to −54.4‰ and from +3.1‰ to +8.7‰, indicating a source of metamorphic fluid.
(2) The $\delta^{34}S$ values for the ore-related pyrites of the Tuwaishan gold deposit are from +4.5‰ to +7.9‰, reflecting a source of metamorphism for the ore-forming materials.
(3) The Tuwaishan and other gold deposits along the Gezhen shear zone are orogenic gold deposit that were formed as a result of regional metamorphism.
(4) The Mesoproterozoic basement rocks could not be the source of the Gezhen gold deposits. Instead, the Ordovician–Silurian rocks on the footwall of the Gezhen shear zone are most likely the source for the Tuwaishan and other gold deposits along the shear zone, even though more work is required to confirm such a source.

Author Contributions: Formal analysis, Y.L.; funding acquisition, D.X. and Y.L.; investigation, Y.L., L.W. and J.H.; writing—original draft, Y.L.; writing—review and editing, J.M. All authors have read and agreed to the published version of the manuscript.

Funding: This research was jointly funded by the National Natural Science Foundation of China (Grant No. U2244219), the National Nonprofit Institute Research Grant of IGGE (AS2022P03), and the Chinese Geological Survey Program (Grant Nos. DD20190047, DD20221807, DD20230013).

Data Availability Statement: All data generated or used during the current study are available in full within this article.

Acknowledgments: We sincerely thank Lingku Meng for the permission of sampling in the Tuwaishan gold mining area. We are grateful to three anonymous reviewers for their constructive comments.

Conflicts of Interest: The authors declare no conflict of interest.

References

1. Metcalfe, I. Gondwana dispersion and Asian accretion: Tectonic and palaeogeographic evolution of eastern Tethys. *J. Asian Earth Sci.* **2013**, *66*, 1–33. [CrossRef]
2. He, H.Y.; Wang, Y.J.; Cawood, P.A.; Qian, X.; Zhang, Y.Z.; Zhao, G.F. Permo–Triassic granitoids, Hainan Island, link to Paleotethyan not Paleopacific tectonics. *Geol. Soc. Am. Bull.* **2020**, *132*, 2067–2083. [CrossRef]
3. Mao, J.W.; Zhou, Z.H.; Feng, C.Y.; Wang, Y.T.; Zhang, C.Q.; Peng, H.J.; Yu, M. A preliminary study of the Triassic large-scale mineralization in China and its geodynamic setting. *Geol. China* **2012**, *39*, 1437–1471.
4. HBG (Hainan Bureau of Geology). *Geology of Hainan Province*; Geological Publishing House: Beijing, China, 2017; pp. 844–853.
5. Xu, D.R.; Wang, Z.L.; Wu, C.J.; Zhou, Y.Q.; Shan, Q.; Hou, M.Z.; Fu, Y.R.; Zhang, X.W. Mesozoic gold mineralization in Hainan Province of South China: Genetic types, geological characteristics and geodynamic settings. *J. Asian Earth Sci.* **2017**, *137*, 80–108. [CrossRef]
6. Goldfarb, R.; Qiu, K.F.; Deng, J.; Chen, J.; Yang, L.Q. Orogenic Gold Deposits of China. *Econ. Geol.* **2019**, *22*, 263–324. [CrossRef]
7. Goldfarb, R.J.; Mao, J.W.; Qiu, K.F.; Goryachev, N. The great Yanshanian metallogenic event of eastern Asia: Consequences from one hundred million years of plate margin geodynamics. *Gondwana Res.* **2022**, *100*, 223–250. [CrossRef]
8. Liu, Y.H.; Mao, J.W.; Miggins, D.P.; Qiu, K.F.; Hu, J.; Wang, L.; Xu, D.M.; Goldfarb, R.J. 40Ar/39Ar geochronology constraints on formation of the Tuwaishan orogenic gold deposit, Hainan Island, China. *Ore Geol. Rev.* **2020**, *120*, 103438. [CrossRef]
9. Zhang, F.F.; Wang, Y.J.; Chen, X.Y.; Fan, W.M.; Zhang, Y.H.; Zhang, G.W.; Zhang, A.M. Triassic high-strain shear zones in Hainan Island (South China) and their implications on the amalgamation of the Indochina and South China Blocks: Kinematic and 40Ar/39Ar geochronological constraints. *Gondwana Res.* **2011**, *19*, 910–925. [CrossRef]
10. Liang, X.Q. Geology and genesis of the Tuwaishan gold ore deposit in Hainan Province of South China. *Reg. Geol. China* **1992**, *2*, 174–182.
11. Chen, Z.Z.; Yu, S.J.; Chen, B.H.; Qing, L. Geological characteristics and genesis of the Baoban gold ore belt in Hainan Island of South China. *Miner. Depos.* **1993**, *12*, 318–348.
12. Tu, S.X.; Gao, Y.J. Ore-forming fluids and stable isotope geochemistry of several gold deposits in southwestern Hainan Island. *Miner. Depos.* **1993**, *12*, 338–348.
13. Yang, G.Q.; Mao, J.W.; Lu, L.; Liu, J.; Yang, J. Characteristics of Fluid Inclusion in the Tuwaishan Gold Deposit, Hainan Province and Their Geological Significances. *Acta Geol. Sin.* **2008**, *82*, 1540–1546.

14. Huang, X.D.; Ding, S.J. Genesis and geology and geochemistry of Erjia gold deposit, Western Hainan. *Contr. Geol. Miner. Resour. Res.* **1992**, *7*, 24–34.
15. Xia, Y.; Wu, X.Y.; Yang, Y.G. The fluid inclusion studies of gold deposits in Gezhen shear zone Hainan, China. *Geochimica* **1995**, *24*, 160–167. [CrossRef]
16. Hou, W.; Chen, H.F.; Wang, K.F.; Peng, G.L.; Tang, H.F.; Liang, X.Q.; Xu, D.R. *Geotectonics of Hainan Island and Its Gold Metallogeny*; Science Press: Beijing, China, 1996; pp. 1–229.
17. Xia, Y. Isotope geochemistry of gold mineralization in Gezhen shear zone, Hainan, China. *J. Guizhou Univ. Technol. (Nat. Sci. Ed.)* **2002**, *31*, 18–23.
18. Li, Z.X.; Li, X.H.; Zhou, H.W.; Kinny, P. Grenvillian continental collision in south China: New SHRIMP U-Pb zircon results and implications for the configuration of Rodinia. *Geology* **2002**, *30*, 163–166. [CrossRef]
19. Yao, W.H.; Li, Z.X.; Li, W.X.; Li, X.H. Proterozoic tectonics of Hainan Island in supercontinent cycles: New insights from geochronological and isotopic results. *Precambrian Res.* **2017**, *290*, 86–100. [CrossRef]
20. Zhang, L.M.; Wang, Y.J.; Qian, X.; Zhang, Y.Z.; He, H.Y.; Zhang, A.M. Petrogenesis of Mesoproterozoic mafic rocks in Hainan (South China) and its implication on the southwest Hainan-Laurentia-Australia connection. *Precambrian Res.* **2018**, *313*, 119–133. [CrossRef]
21. Zhang, L.M.; Zhang, Y.Z.; Cui, X.; Cawood, P.A.; Wang, Y.J.; Zhang, A.M. Mesoproterozoic rift setting of SW Hainan: Evidence from the gneissic granites and metasedimentary rocks. *Precambrian Res.* **2019**, *325*, 69–87. [CrossRef]
22. Xu, Y.J.; Cawood, P.; Zhang, H.C.; Zi, J.W.; Zhou, J.B.; Li, L.X.; Du, Y.-S. The Mesoproterozoic Baoban Complex, South China: A missing fragment of western Laurentian lithosphere. *Geol. Soc. Am. Bull.* **2019**, *132*, 1404–1418. [CrossRef]
23. Phillips, G.N.; Powell, R. Formation of gold deposits: A metamorphic devolatilization model. *J. Metamorph. Geol.* **2010**, *28*, 689–718. [CrossRef]
24. Tomkins, A.G. Windows of metamorphic sulfur liberation in the crust: Implications for gold deposit genesis. *Geochim. Cosmochim. Acta.* **2010**, *74*, 3246–3259. [CrossRef]
25. Deng, J.; Yang, L.Q.; Groves, D.I.; Zhang, L.; Qiu, K.F.; Wang, Q.F. An integrated mineral system model for the gold deposits of the giant Jiaodong province, eastern China. *Earth-Sci. Rev.* **2020**, *208*, 103274. [CrossRef]
26. Deng, J.; Wang, Q.F.; Liu, X.F.; Zhang, L.; Yang, L.Q.; Yang, L.; Qiu, K.F.; Guo, L.N.; Liang, Y.Y.; Ma, Y. The Formation of the Jiaodong Gold Province. *Acta Geol. Sin. (Engl. Ed.)* **2022**, *96*, 1801–1820. [CrossRef]
27. Qiu, K.F.; Deng, J.; Laflamme, C.; Long, Z.Y.; Wan, R.Q.; Moynier, F.; Yu, H.C.; Zhang, J.Y.; Ding, Z.J.; Goldfarb, R. Giant Mesozoic gold ores derived from subducted oceanic slab and overlying sediments. *Geochim. Cosmochim. Acta* **2023**, *343*, 133–141. [CrossRef]
28. Yu, H.C.; Qiu, K.F.; Sai, S.X.; McIntire, D.C.; Pirajno, F.; Duo, D.W.; Miggins, D.P.; Wang, J.; Jia, R.Y.; Wu, M.Q. Paleo-tethys late triassic orogenic gold mineralization recorded by the Yidi'nan gold deposit, West Qinling, China. *Ore Geol. Rev.* **2020**, *116*, 103211. [CrossRef]
29. Wang, Y.J.; Qian, X.; Cawood, P.A.; Liu, H.C.; Feng, Q.L.; Zhao, G.C.; Zhang, Y.H.; He, H.Y.; Zhang, P.Z. Closure of the East Paleotethyan Ocean and amalgamation of the Eastern Cimmerian and Southeast Asia continental fragments. *Earth-Sci. Rev.* **2018**, *186*, 195–230. [CrossRef]
30. Dilek, Y.; Tang, L. Magmatic record of the Mesozoic geology of Hainan Island and its implications for the Mesozoic tectono-magmatic evolution of SE China: Effects of slab geometry and dynamics in continental tectonics. *Geol. Mag.* **2020**, *158*, 118–142. [CrossRef]
31. Deng, J.; Wang, Q.; Sun, X.; Yang, L.; Groves, D.I.; Shu, Q.; Gao, L.; Yang, L.; Qiu, K.; Wang, C. Tibetan ore deposits: A conjunction of accretionary orogeny and continental collision. *Earth-Sci. Rev.* **2022**, *235*, 104245. [CrossRef]
32. Qiu, K.F.; Deng, J.; Sai, S.X.; Yu, H.C.; Tamer, M.T.; Ding, Z.J.; Yu, X.F.; Goldfarb, R. Low-Temperature Thermochronology for Defining the Tectonic Controls on Heterogeneous Gold Endowment Across the Jiaodong Peninsula, Eastern China. *Tectonics* **2023**, *42*, e2022TC007669. [CrossRef]
33. Yu, H.C.; Qiu, K.F.; Deng, J.; Zhu, R.; Mathieu, L.; Sai, S.X.; Sha, W.J. Exhuming and preserving epizonal orogenic Au-Sb deposits in rapidly uplifting orogenic settings. *Tectonics* **2022**, *41*, e2021TC007165. [CrossRef]
34. Liang, X.Q.; Hou, W.; Chen, H.F. Gezhen brittle and ductile superimposition shear zone in Hainan Island. *Geotect. Metall.* **1990**, *14*, 254–263.
35. Ding, S.J. The tectonic evolution of the Gezhen fault zone and its gold mineralization series. *Contr. Geol. Miner. Resour. Res.* **1994**, *9*, 1–8.
36. Zhan, M.G.; Zhang, S.H.; Liu, G.Q. The Gezhen auriferous shear zone and related gold ore system in western Hainan Island of South China. *Miner. Depos.* **1996**, *15*, 289–297.
37. Ma, D.Q.; Wang, X.D.; Chen, Z.P.; Xiao, Z.F.; Zhang, W.C.; Zhong, S.Z. New achievements about Baoban Group in Hainan Island. *Reg. Geol. China* **1997**, *16*, 130–136.
38. Chen, X.Y.; Wang, Y.J.; Fan, W.M.; Peng, T.P.; Ge, T.H. Microstructure characteristics of NE trend ductile shear zones of southwestern Hainan: Constraints from 40Ar-39Ar geochronology. *Geochimica* **2006**, *35*, 479–488.
39. Xu, D.R.; Xia, B.; Li, P.C.; Zhang, Y.Q.; Chen, G.H.; Ma, C. SHRIMP U-Pb dating on zircon from the Precambrian granitoid rock in northwest Hainan Island and its geological implications. *Geotecton. Metallog.* **2006**, *30*, 510–518.
40. Liu, Y.H.; Mao, J.W.; Qiu, K.F.; Hu, J.; Wang, L.; Xu, D.M. Extensional Setting of Hainan Island in Mesoproterozoic: Evidence from Granitic Intrusions in the Baoban Group. *Acta Geol. Sin. (Engl. Ed.)* **2022**, *96*, 1199–1212. [CrossRef]

41. Ma, D.Q.; Huang, X.D.; Xiao, Z.F.; Chen, Z.P.; Zhang, W.C.; Zhong, S.Z. *Crystallized Basement in Hainan Island: Sequence and Epoch of the Baoban Group*; China University of Geosciences Press: Beijing, China, 1998; pp. 1–52.
42. Chen, Z.P. *Petrostratigraphy in Hainan Province*; Geological Publishing House: Beijing, China, 1997; pp. 844–853.
43. Wen, S.N. Geochronologic and Geochemical Studies of Permian-Triassic Magmatism in Hainan Island, South China. Ph.D. Thesis, University of Chinese Academy of Sciences, Guangzhou, China, 2013.
44. Song, H.X. Mesoproterozoic Mafic Magmatism and Its Geological Significances on Hainan Island. Master's Thesis, Guilin University of Technology, Guilin, China, 2022.
45. Xu, D.R.; Wang, Z.L.; Cai, J.X.; Wu, C.J.; Bakun-Czubarow, N.; Wang, L.; Chen, H.Y.; Baker, M.J.; Kusiak, M.A. Geological characteristics and metallogenesis of the shilu Fe-ore deposit in Hainan Province, South China. *Ore Geol. Rev.* **2013**, *53*, 318–342. [CrossRef]
46. Peng, S.M.; Ding, S.J. Isotopic features of the Gezhen gold ore zone in Hainan Province of South China, and their geological significance. *Gold* **1993**, *14*, 6–12.
47. Liu, Y.H.; Li, B.L.; Cao, X.; Luo, M.C.; Zhou, W.L. Ore-forming fluid characteristics of the Jinchang gold deposit in Hainan Island of China and its constraint on ore genesis. *Acta Geol. Sin.* **2015**, *89*, 755–765.
48. Ltd, H.J.G. Summary Report on Geological Exploration and Deep Exploration in Tuwaishan Gold Mine Area. 2017; pp. 78–88.
49. Sai, S.X.; Deng, J.; Qiu, K.F.; Miggins, D.P.; Zhang, L. Textures of auriferous quartz-sulfide veins and 40Ar/39Ar geochronology of the Rushan gold deposit: Implications for processes of ore-fluid infiltration in the eastern Jiaodong gold province, China. *Ore Geol. Rev.* **2020**, *117*, 103254. [CrossRef]
50. Qiu, K.F.; Deng, J.; He, D.Y.; Rosenbaum, G.; Zheng, X.; Williams-Jones, A.E.; Yu, H.C.; Balen, D. Evidence of vertical slab tearing in the Late Triassic Qinling Orogen (central China) from multiproxy geochemical and isotopic imaging. *J. Geophys. Res. Solid Earth* **2023**, *128*, e2022JB025514. [CrossRef]
51. Coleman, M.L.; Shepherd, T.J.; Durham, J.J.; Rouse, J.E.; Moore, G.R. Reduction of water with zinc for hydrogen isotope analysis. *Anal. Chem.* **1982**, *54*, 993–995. [CrossRef]
52. Clayton, R.N.; Mayeda, T.K. The use of bromine pentafluoride in the extraction of oxygen from oxides and silicates for isotopic analysis. *Geochim. Cosmochim. Acta.* **1963**, *27*, 43–52. [CrossRef]
53. Taylor, H.P. The Application of Oxygen and Hydrogen Isotope Studies to Problems of Hydrothermal Alteration and Ore Deposition. *Econ. Geol.* **1974**, *69*, 843–883. [CrossRef]
54. Goldfarb, R.J.; Groves, D.I. Orogenic gold: Common or evolving fluid and metal sources through time. *Lithos* **2015**, *233*, 2–26. [CrossRef]
55. Xiao, Z.F. Study on Metallogenic Mechanism of the Baoban-Tuwaishan Gold Deposits on Hainan Island. Master's Thesis, Institute of Geochemistry, Chinese Academy of Sciences, Guiyang, China, 1989.
56. Feng, L.S. Study on isotopic and geological characteristics of Baoban gold deposit in Hainan Island. *Geol. Resour.* **1989**, *3*, 41–47.
57. Chen, H.S. Geochemical Tracer Studies on the Isotopes from the Gold Deposits, Hainan. *Acta Geosci. Sin.* **1996**, *17*, 302–312.
58. Chen, S.M.; Zhou, Y.X.; Li, B.; Wu, J.H.; Zhao, H.T.; Zhang, Z.M.; Zeng, H. Genesis of Chaxi Gold Deposit in Southwestern Hunan Province, Jiangnan Orogen (South China): Constraints from Fluid Inclusions, H-O-S-Pb Isotopes, and Pyrite Trace Element Concentrations. *Minerals* **2022**, *12*, 867. [CrossRef]
59. Li, J.; Ren, Y.; Yang, Q.; Sun, X. Ore Genesis of the Toudaochuan Gold Deposit in Central Jilin Province, NE China: Constraints from Fluid Inclusions and C–H–O–S–Pb Isotopes. *Minerals* **2022**, *12*, 964. [CrossRef]
60. Qiu, K.F.; Yu, H.C.; Hetherington, C.; Huang, Y.Q.; Yang, T.; Deng, J. Tourmaline composition and boron isotope signature as a tracer of magmatic-hydrothermal processes. *Am. Miner.* **2021**, *106*, 1033–1044. [CrossRef]
61. Qiu, K.F.; Yu, H.C.; Deng, J.; McIntire, D.; Gou, Z.Y.; Geng, J.Z.; Chang, Z.S.; Zhu, R.; Li, K.N.; Goldfarb, R. The giant Zaozigou Au-Sb deposit in West Qinling, China: Magmatic- or metamorphic-hydrothermal origin? *Miner. Depos.* **2020**, *55*, 345–362. [CrossRef]
62. Goldfarb, R.J.; Pitcairn, I. Orogenic gold: Is a genetic association with magmatism realistic? *Miner. Depos.* **2022**, *58*, 5–35. [CrossRef]
63. Xiao, Z.F.; Ouyang, Z.Y.; Lu, H.Z.; Guha, Y. Fluid inclusion geochemical study on the Baoban gold field, Hainan Island, South China. *Miner. Depos.* **1994**, *13*, 172–180.
64. Chen, Y.J.; Ni, P.; Fan, H.R.; Pirajno, F.; Lai, Y.; Su, W.C.; Zhang, H. Diagnostic fluid inclusions of different types hydrothermal gold deposits. *Acta Geosci. Sin.* **2007**, *23*, 2085–2108.
65. Ridley, J.R.; Diamond, L.W. Fluid chemistry of orogenic lode gold deposits and implications for genetic models. *Rev. Econ. Geol.* **2000**, *13*, 141–162.
66. Zhang, Z.H.; Mao, J.W.; Wang, Y. Characteristics of fluid inclusions in the gold deposits within Zhongchuan area, western Qinling and their geological significance. *Acta Petrol. Miner.* **2004**, *23*, 147–157.
67. Zhang, Z.H.; Mao, J.W.; Wang, Z.L.; Zuo, G.C.; Chen, W.S.; Zhu, H.P.; Wang, L.S.; Lv, L.S. Geochemistry of fluid inclusions in the Axi gold deposit, West Tianshan, Xinjiang. *Acta Geosci. Sin.* **2007**, *23*, 2403–2414.
68. Yang, Y.G.; Wu, X.Y. Study on Geology and Geochemistry of the Erjia gold deposit in Hainan Island. *Gold Sci. Technol.* **1995**, *3*, 19–25.
69. Ohmoto, H. Systematics of Sulfur and Carbon Isotopes in Hydrothermal Ore Deposits. *Econ. Geol.* **1972**, *67*, 551–578. [CrossRef]
70. Seal, R.R. Sulfur Isotope Geochemistry of Sulfide Minerals. *Rev. Mineral. Geochem.* **2006**, *61*, 633–677. [CrossRef]

71. Wang, S.; Liu, Z.J.; Liu, Y.H.; Deng, N.; Yang, B.Z.; Tan, L. Contribution of Triassic Tectonomagmatic Activity to the Mineralization of Liziyuan Orogenic Gold Deposits, West Qinling Orogenic Belt, China. *Minerals* **2023**, *13*, 130. [CrossRef]
72. Long, Z.Y.; Qiu, K.F.; Santosh, M.; Yu, H.C.; Jiang, X.Y.; Zou, L.Q.; Tang, D.W. Fingerprinting the metal source and cycling of the world's largest antimony deposit in Xikuangshan, China. *Geol. Soc. Am. Bull.* **2023**, *135*, 286–294. [CrossRef]
73. Qiu, K.F.; Goldfarb, R.J.; Deng, J.; Yu, H.C.; Gou, Z.Y.; Ding, Z.J.; Wang, Z.K.; Li, D.P. Gold Deposits of the Jiaodong Peninsula, Eastern China. *SEG Spec. Publ.* **2020**, *23*, 753–774.
74. Goldfarb, R.J.; Baker, T.; Dube, B.; Groves, D.I.; Hart, C.J.R.; Gosselin, P. Distribution, Character, and Genesis of Gold Deposits in Metamorphic Terranes. In *Economic Geology 100th Anniversary Volume*; Society of Economic Geologists: Littleton, CO, USA, 2005; pp. 407–450.
75. Phillips, G.N.; Powell, R. Formation of gold deposits: Review and evaluation of the continuum model. *Earth-Sci. Rev.* **2009**, *94*, 1–21. [CrossRef]
76. Tomkins, A.G.; Catherine, G. Upper Temperature Limits of Orogenic Gold Deposit Formation: Constraints from the Granulite-Hosted Griffin's Find Deposit, Yilgarn Craton. *Econ. Geol.* **2009**, *104*, 669–685. [CrossRef]
77. Zhong, R.C.; Brugger, J.; Tomkins, A.G.; Chen, Y.J.; Li, W.B. Fate of gold and base metals during metamorphic devolatilization of a pelite. *Geochim. Cosmochim. Acta* **2015**, *171*, 338–352. [CrossRef]
78. Yu, H.C.; Qiu, K.F.; Nassif, M.T.; Geng, J.Z.; Sai, S.X.; Duo, D.W.; Huang, Y.Q.; Wang, J. Early orogenic gold mineralization event in the West Qinling related to closure of the Paleo-Tethys Ocean–Constraints from the Ludousou gold deposit, central China. *Ore Geol. Rev.* **2020**, *117*, 103217. [CrossRef]